

Received December 25, 2018; reviewed; accepted November 13, 2019

Study on the floc-bubble adhesion behavior of hematite in static flow field

Jinxia Zhang, Hongjun Feng, Fusheng Niu, Weiguang Sun, Yawei Zhao

College of Mining Engineering, North China University of science and technology, Tangshan 063210, China;

Corresponding author: niufusheng@126.com (Fusheng Niu)

Abstract: To investigate the adhesion of hematite flocs to gas bubbles in floc floatation, this paper develops an observation system for floc-bubble collision and adhesion with two charge-coupled device (CCD) cameras. The sizes of flocs and bubble were 45.36 μm and 0.90mm, respectively, and the distance between a floc and the bubble center (sedimentation distance) was set to 0.25cm. Three surfactants, namely, sodium oleate, lauryl amine and sodium dodecyl sulfate (SDS), were selected for our research. Several experiments were conducted to disclose how surfactant concentration and pH affect the surface adhesion between hematite flocs and bubbles. Then, the adhesion mechanism was discussed in details based on the experimental results. The results show that the highest adhesion probability was achieved for the said floc and bubble at the lauryl amine concentration of 8mg/L, the sedimentation distance of 0.25cm and the pH of 9. After touching the bubble, the hematite floc slid on the bubble surface, forming a stable three-phase interface after 67ms. Then, the radial position of the floc no longer changed, despite the floc motion on the bubble surface. According to the Derjaguin-Landau-Verwey-Overbeek (DLVO) theory and the potential energy of the van der Waals force, there was a repulsive force between the floc and the bubble in the absence of surfactant and an attractive force in the presence of the surfactant of lauryl amine. In addition, a thin solvation shell is conducive to the adhesion between the floc and the bubble.

Keywords: bubble, floc, adhesion, charge-coupled device (CCD) camera, Derjaguin-Landau-Verwey-Overbeek (DLVO) theory

1. Introduction

With the rapid depletion of easily-exploitable coarse-grained minerals, the efficient recovery of fine-grained ($-10\mu\text{m}$) minerals has become a hot issue in the beneficiation industry. Floc floatation is considered a promising technique for the recovery of fine mineral particles (Sivamohan, 1990; Song et al., 2007; Shahbaziet al., 2010; Ahmadiet al., 2014). During floc floatation, the air is introduced as small bubbles (size: 0.1~4mm) to serve as the carrier. The air bubbles will collide with the suspended floc particles and the latter will selective adhere to the bubbles, forming a stable bubble-particle aggregate with good separation effect (Jorgeet al., 1993; Nguyen et al., 2004). The collision and adhesion, being the key to floc floatation, have attracted much attention from the academia (Wuet al., 2018; Tian et al., 2017). The relevant research has yielded fruitful testing and theoretical results (Jameson et al., 1977; Schulze, 1989; Nguyen, 1999). Overall, scholars at home and abroad mainly tackle the bubble-particle collision, especially the collision probability and the roles of fluids in the collision. However, many experiments have shown that collision is not necessarily followed by the adhesion of particles to the bubbles (Kralchevsky et al., 2009; Nguyen et al., 2003).

Under varied fluid and mechanical forces, the particles and the bubbles move close to each other, and the solvation shells of both become thinner and even burst. Eventually, a stable three-phase wetted interface is formed, including the solid phase, the liquid phase and the gas phase (Koh et al., 2011; Rahman et al., 2014; Zhang et al., 2014). The adhesion of particles to bubbles depends on surface

hydrophobicity and electrical properties, particularly on the thinning and burst of the solvation shells (Jiang et al., 1993; Kouachiet al., 2010). The thinning and burst process was firstly studied by Frumkin in the 1930s (Hassanzadeh et al., 2016). Through the analysis on the thinned solvation shells, Derjayin et al. (1984) concluded that the retention of these shells has no impact on the flotation effect. Schulze and Nguyen (Wang et al., 2003; Nguyen et al., 2004) held that the collision and adhesion between mineral particles and gas bubbles are determined by the burst situation of the solvation shells on the surface of the mineral: after collision, the hydration layer between the flocs, which are hydrophobic on the surface, and the bubbles become thinner and burst; the resulting three-phase interface between gas, liquid and solid will promote the adhesion of flocs to the bubbles.

This paper attempts to explain the adhesion of hematite flocs to gas bubbles in floc floatation. For this purpose, charge-coupled device (CCD) cameras were adopted to build an observation system for floc-bubble collision and adhesion in the lab. The sizes of flocs and bubble were 45.36 μm and 0.90mm, respectively, and the distance between a floc and the bubble center (sedimentation distance) was 0.25cm. Three surfactants were selected, namely, sodium oleate, lauryl amine and sodium dodecyl sulfate (SDS). Several experiments were conducted to disclose how surfactant concentration and pH affect the surface adhesion between hematite flocs and bubbles. Then, the adhesion mechanism was discussed in details based on the experimental results.

2. Materials and methods

2.1. Experimental materials

Hematite was obtained from Sijiaying Iron Mine, northern China's Hebei Province, and made into samples with a purity of 68.50%. Then, hematite flocs were prepared by grounding 3g samples to less than 5 μm , and mixed with self-prepared starch-acrylamide (Fig. 1) in a beaker. The mixture was conditioned for 10min and stirred at 300~400r/min. The mean size of the prepared flocs was 45.36 μm (Fig. 2). The physical properties of the flocs were analyzed and recorded in Table 1. The prepared hematite flocs were subjected to physical property analysis as shown in Table 1.

Table 1. Physical properties of the flocs

Flocs size/ μm	Flocsdensity /g cm ³	Flocs porosity /%	Flocs fractal dimension	The projection area of flocs/10 ⁻³ mm ²	Flocs strength /Pa mm ²
45.36	3.03	46.19	1.67	1.91	1361.21

Table 2 lists the purities and physicochemical properties of the three surfactants. The critical micelle concentration (CMC) was determined by surface tension method (Cheng et al., 2018), and the hydrophilic-lipophilic balance (HLB) was calculated by Griffin's method (Griffin et al., 2015; Wang et al., 2016). The experimental solutions were prepared with fresh deionized water at 20°C.

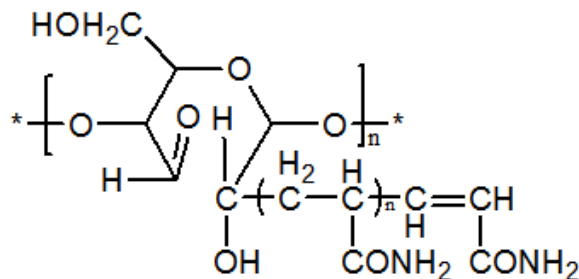


Fig. 1. Molecular structure of self-prepared starch-acrylamide

2.2. Experiment device

The observation system for floc-bubble collision and adhesion is illustrated in Fig. 3. The system mainly consists of a Vernier device, an observation room (size: 15 cm×15 cm×30 cm), two CCD cameras (dual lens; effective pixels: 768×493; magnification: 0.75~4.50), a steel capillary tube (inner diameter: 0.3~0.6

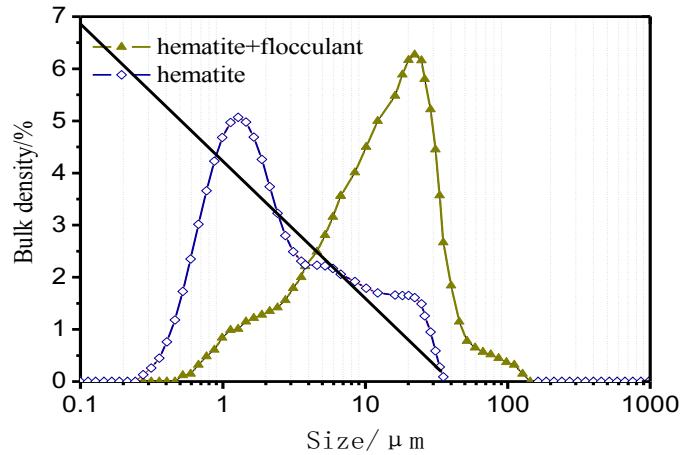


Fig. 2. Mean size of the prepared flocs

Table 2. Purities and physicochemical properties of surfactants

Surfactant	Polarity	Molecular weight	Purity/%	CMC / (mol/L)	HLB
SDS	Anion	288.372	98.50	0.0090	12.3
Lauryl amine	Kation	185.35	98.00	0.0050	2.9
Sodium oleate	Anion	304.44	99.95	0.0048	18.0

mm) a Pasteur pipet, a halogen light source, a computer, and a metal stand. The observation room is a transparent plexiglass tank.

2.3. Experiment and analysis methods

Once the adjustment was completed, the hematite floc slurries were slowly dripped into the observation room filled with deionized water. Based on the falling trajectories of the flocs (Fig. 4), the adhesion status of the flocs falling from different positions to the bubble was determined. Meanwhile, the relative movement between the flocs and the bubble was captured by the CCD cameras. The dripping process under each experimental condition were shot three times to enhance the data reliability.

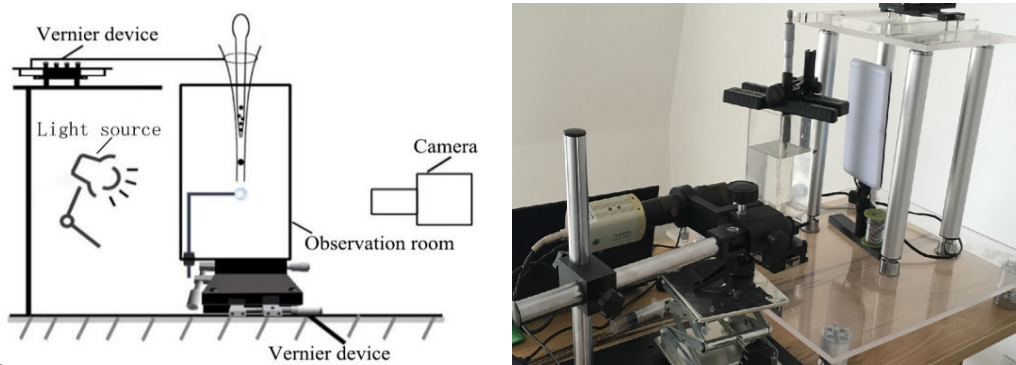


Fig. 3. Sketch map of the observation system

For simplicity, only those falling from the two edges of the bubble were considered effective particles. The probability P_a for flocs to adhere to the bubble can be computed by:

$$P_a = \frac{N_a}{N_t} \times 100\% \quad (1)$$

where N_a is the number of flocs adhered to the bubble and N_t is the number of flocs dripping from the same position in a static environment.



Fig. 4. Falling trajectories of the flocs



Fig. 5. Screenshots from video tracking cameras

The images on the flocs and the bubble were subjected to grayscale processing and interface extraction by Otsu's method for image segmentation. Firstly, the black and white colors of the images were differentiated, and the target flocs and the target bubble were marked. On this basis, the targets were fitted to a circle, using the least squares method.

To judge floc-bubble adhesion accurately, two images from the video were examined at the same time. The flocs in the first video sequence were tracked before those in the second video sequence. Based on the falling sequence, the initial floc positions and the occurrence/absence of collision and adhesion were displayed directly in the Common Window. Fig. 5 is a screenshot at a time point in the video.

3. Results and discussion

3.1. Effects of surfactant concentration on adhesion

Fig. 6 shows the variation in adhesion probability with sedimentation distances at different concentrations of sodium oleate under $T=25^{\circ}\text{C}$ and $\text{pH}=7$. Obviously, not all flocs falling from right above the bubble center adhered to the bubble; as the falling position moved outward, the adhesion probability gradually decreased; the adhesion probability also changed with the concentrations of sodium oleate.

Fig. 7 presents the adhesion probabilities at different concentrations of sodium oleate, while the sedimentation distance remained unchanged. It can be seen that the adhesion probability exhibited a gradual growth, as the concentration of sodium oleate increased from 4 to 8mg/L, and reached the first peak (55.04%) at the concentration of 8mg/L. Further growth in the concentration caused a decline in the adhesion probability. When the amount climbed to 20mg/L, the adhesion probability dropped to 41.60%. Hence, the neutral or weak alkaline environment is favorable for floc-bubble adhesion, if sodium oleate serves as the surfactant.

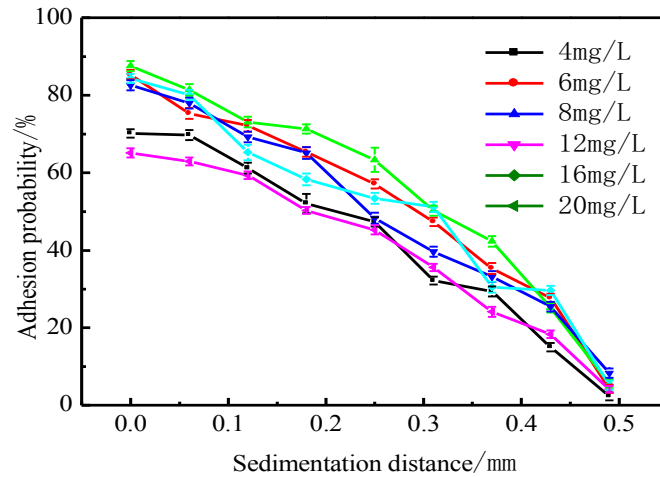


Fig. 6. The variation in adhesion probability with sedimentation distances at different concentrations of sodium oleate

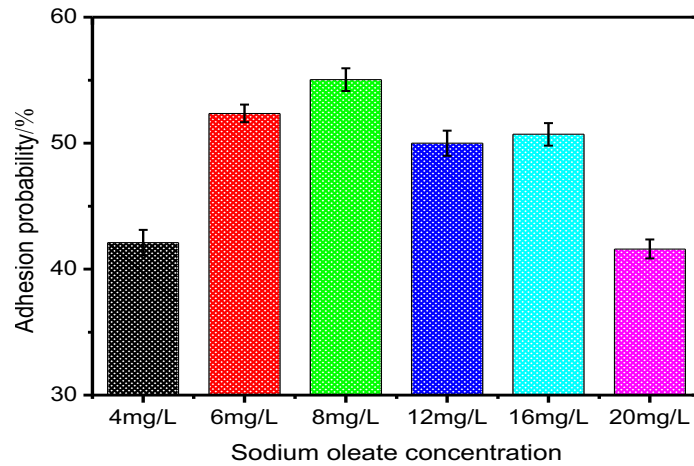


Fig. 7. The adhesion probabilities at different concentrations of sodium oleate

3.2. Effects of surfactant type on adhesion

Fig. 8 compares the adhesion probabilities under the three surfactants, i.e. sodium oleate, lauryl amine and the SDS, when all of them were at the same concentration (8mg/L). As shown in Fig. 8, as the falling position moved outward, the adhesion probabilities under the three surfactants all decreased, but at different rates. For example, under the sedimentation distance of 0.25mm, the adhesion probabilities were 25.31%, 63.36% and 64.78%, respectively, in the SDS solution, the sodium oleate solution and the lauryl amine solution.

It can also be observed from the experiment that the flocs quickly left the bubble after collision under the three surfactants. Even if they adhered to the bubble, the flocs soon slid away from the bottom of the bubble under the gravitational force, due to the extremely weak adhesive force. Relatively, the hematite floc-bubble adhesion was the most prominent under the cationic surfactant of lauryl amine.

3.3. Effects of lauryl amine concentration on adhesion

Fig. 9 displays the variation in the adhesion probability with the concentrations of lauryl amine under $T=25^{\circ}\text{C}$ and $\text{pH}=7$. It is learned that the adhesion probability changed greatly with the lauryl amine concentrations and with the sedimentation distances. As the concentration grew to 8mg/L, the adhesion probability continued to increase. However, the adhesion probability started to decline slowly, once the concentration surpassed 8mg/L. This means properly increasing the lauryl amine concentration can promote the floc-bubble adhesion.

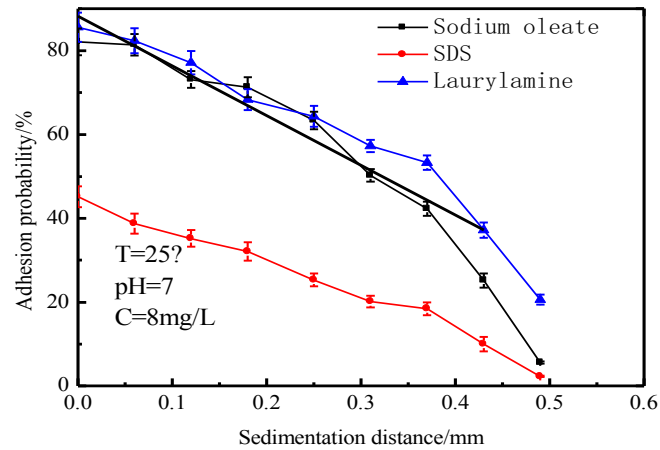


Fig. 8. The adhesion probabilities under the three surfactants

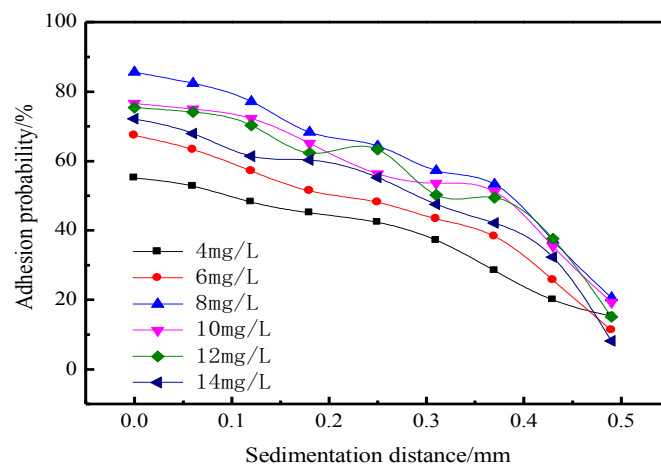


Fig. 9. The variation in the adhesion probability with lauryl amine concentrations and sedimentation distances

3.4. Effects of pH on adhesion under lauryl amine

Fig. 10 shows the adhesion probabilities at different pH values (i.e. 1, 3, 5, 7, 9, 11 and 13), under the lauryl amine concentration of 8mg/L and $T=25^{\circ}\text{C}$. As shown in Fig. 10, whichever the pH, the adhesion probability is negatively correlated with the sedimentation distance. In addition, the adhesion probability of the hematite flocs after collision was higher at the pH of 9 at any falling position than that at any other pH value.

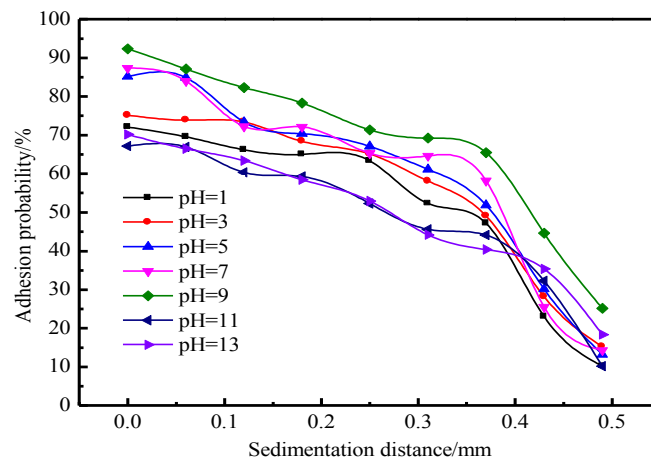


Fig. 10. The adhesion probabilities at different pH values

4. Analysis on adhesion mechanism

4.1. Floc movement on bubble surface

Fig. 11 shows how an irregular hematite floc moved on the bubble surface under lauryl amine, after it got in touch with the bubble. The bubble diameter (D_b) is 0.90mm, and the floc diameter (D_p) is 45.36 μ m. The 2D images in this figure were captured by the CCD cameras, because the relevant processes (e.g. the floc approaching the bubble and the burst of solvation shell) all occurred in milliseconds. As shown in the figure, there was a protrusion on the floc surface, whose position changed as the floc moved on the bubble surface; once it touched the bubble, the floc slid from the top to the bottom of the bubble and eventually stabilized.



Fig. 11. Motion of an irregular hematite floc on the bubble surface

4.2. Change of floc positions on bubble surface

As the floc approached and collided into the bubble, its position changed both in the radial and axial directions relative to the bubble. These changes were plotted and displayed as Fig. 12. In the light of this figure, the floc motion could be divided into three phases:

(1) Before collision, the radial position of the floc changed rapidly. In this phase, the floc simply sedimented in the solution (Area I).

(2) After touching the bubble, the floc slowed down and its radial position remained unchanged for a while. In this phase, the part of the floc in contact with the bubble was wrapped by the solvation shell, and the floc started to slide on the interface between it and the bubble (Area II).

(3) Once the solvation shell burst, the three phases, i.e. gas, liquid and solid, contacted with each other. In this phase, the floc's radial position changed instantaneously at about 67ms. Then, a stable three-phase interface emerged, and the radial position no longer changed with the sliding process (Area III).

4.3. Analysis on adhesion effect

Whether an approaching floc could collide with and adhere to a bubble is determined by the attractive and repulsive forces between the two objects, including but not limited to the van der Waals force, the hydration force and the electrostatic force. Under the combined effects of these forces, the floc sliding on the bubble surface will adhere to or leave from the bubble.

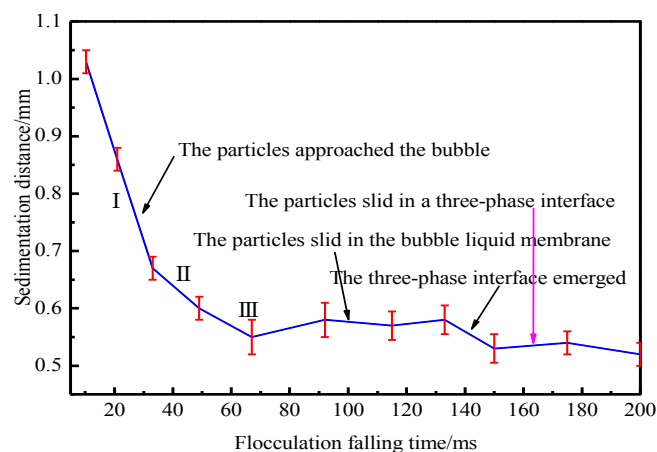


Fig. 12. Relationship between floc falling time and sedimentation distance

Without considering the surfactant, the particle-bubble interaction, which is critical to the floc flotation of ores, is relatively simple. The interaction is mainly affected by the van der Waals force. Most particles will move away from the bubble immediately after the collision, showing a low adhesion probability. If no surfactant is added, the potential energy of van der Waals on the floc and the bubble can be expressed as:

$$U_w = -\frac{K}{6S} \cdot \frac{R_p R_b}{R_p + R_b} \quad (2)$$

where S is the sedimentation distance; R_p is floc size; R_b is the bubble size; K is the Hamaker constant between the floc and the bubble:

$$K = \sqrt{(K_{11} + K_{33} - 2K_{13})(K_{22} + K_{33} - 2K_{23})} = (\sqrt{K_{11}} - \sqrt{K_{33}})(\sqrt{K_{22}} - \sqrt{K_{33}}) \quad (3)$$

where K_{11} , K_{22} and K_{33} are the Hamaker constants for the actions of floc and the bubble and water in the vacuum; K_{13} , K_{23} are the Hamaker constants for floc-water interaction, bubble-water interaction and floc-bubble interaction, respectively.

Substituting $K_{11}=7.60 \times 10^{-20}$ J, $K_{22}=0$, $K_{33}=3.30 \times 10^{-20}$ J, $R_p=45.36 \mu\text{m}$, and $R_b=0.90 \text{mm}$ into the above formulas, we have:

$$K = (\sqrt{7.6} - \sqrt{3.3}) \times \sqrt{3.3} \times 10^{-20} \text{ J} = 1.71 \times 10^{-20} \text{ J}$$

The value of K is negative, indicating that the floc was subjected to a repulsive force. Then, the van der Waals force curve between the floc and the bubble without surfactant (Fig. 13) was obtained by substituting the value of K into formula (2). As shown in Fig. 13, without surfactant, the potential energy between the floc and the bubble was positive. Thus, there was a repulsive force between the floc and the bubble, and the repulsive potential energy decreased with the sedimentation distance. This further hampers the floc-bubble adhesion. As a result, the floc could hardly adhere to the bubble in the absence of surfactant.

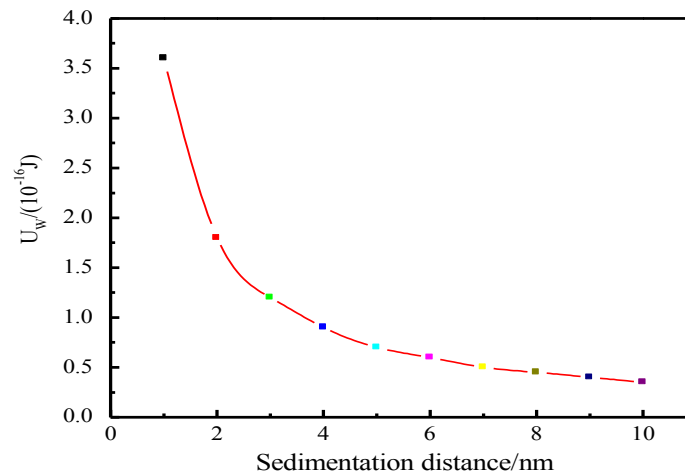


Fig. 13. The van der Waals force curve between the floc and the bubble without surfactant

However, surfactant and other reagents are necessary in actual floc flotation of ores. Once added, the surfactant will be adsorbed onto the floc, changing the floc thickness and the floc-bubble interface. Then, the Hamaker constants will change accordingly. In this case, the potential energy of van der Waals between the floc and the bubble can be expressed as:

$$u_w = \frac{R_p R_b}{6(R_p + R_b)} \cdot \left(\frac{K_1}{S_1} + \frac{K_2}{S_2} + \frac{K_3}{S_3} \right) \quad (4)$$

where:

$$K_1 = (\sqrt{K_d} - \sqrt{K_c})(\sqrt{K_e} - \sqrt{K_c}) \quad (5)$$

$$K_2 = (\sqrt{K_d} - \sqrt{K_a})(\sqrt{K_e} - \sqrt{K_c}) \quad (6)$$

$$K_3 = (\sqrt{K_d} - \sqrt{K_c})(\sqrt{K_b} - \sqrt{K_e}) \quad (7)$$

$$K_4 = (\sqrt{K_d} - \sqrt{K_a})(\sqrt{K_b} - \sqrt{K_e}) \quad (8)$$

$$S_1 = S \cdot S_2 = S + \sigma_1 S_3 = S + \sigma_2 S_4 = S + \sigma_1 + \sigma_1 \quad (9)$$

where K_a , K_b , K_c , K_d and K_e are the Hamaker constants of the floc, the bubble, water, the adsorbed layer on floc surface and the adsorbed layer on bubble surface, respectively. Here, $K_a=20.6 \times 10^{-20} \text{J}$, $K_b=0$ and $K_c=3.3 \times 10^{-20} \text{J}$. If lauryl amine is used as the surfactant, the thicknesses of the two adsorbed layers will become $\sigma_1=\sigma_2=1 \text{nm}$ and 2nm and the corresponding Hamaker constants $K_d=K_e=4.5 \times 10^{-20} \text{J}$.

On this basis, the variations in the potential energy of van der Waals force for the floc and the bubble under the lauryl amine were captured and displayed in Fig. 14. It can be seen that the potential energy of van der Waals force for the floc-bubble interaction was negative. According to the Derjaguin-Landau-Verwey-Overbeek (DLVO) theory, the result means the two objects are mutually attractively. Moreover, the potential energy of the solvation shell was below zero, however the thickness of the shell. This means the attractive force increased as the floc approached the bubble. The absolute value of the potential energy of van der Waals force for the thick shell was smaller than that of the thin shell. Hence, an excessively high concentration of lauryl amine suppresses the floc-bubble adhesion.

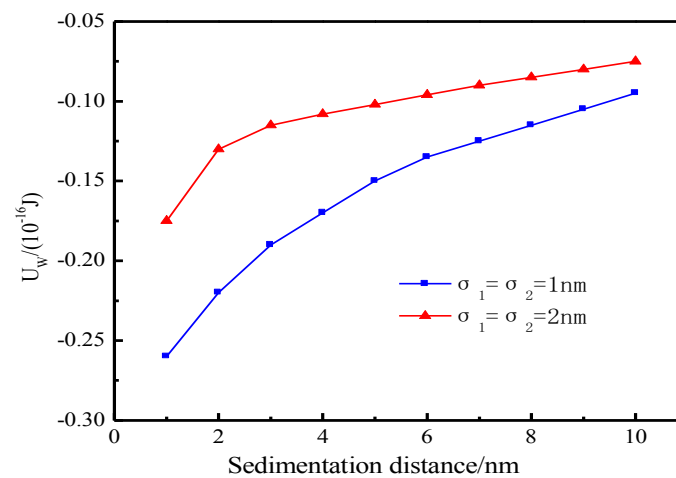


Fig. 14. The variations in the potential energy of van der Waals force under the lauryl amine

5. Conclusions

In this paper, two CCD cameras are adopted to build an observation system for the collision and adhesion between hematite flocs and bubbles in the lab. With this system, the author explored the effects of surfactant concentration, surfactant type and pH value on the adhesion in the static flow field. For the floc size of $45.36 \mu\text{m}$ and the bubble size of 0.90mm , the optimal parameters for adhesion were determined as lauryl amine concentration, 8mg/L ; sedimentation distance, 0.25cm ; pH, 9.

In addition, the adhesion mechanism was investigated in details, revealing that the potential energy of the van der Waals potential energy was positive in the absence of surfactant (i.e. there existed a repulsive force between the floc and the bubble), and turned negative (i.e. the repulsive force became attractive) after the addition of lauryl amine. The absolute value of the potential energy of van der Waals force for the thick solvation shell was smaller than that of the thin shell. Hence, an excessively high concentration of lauryl amine suppresses the floc-bubble adhesion.

Acknowledgments

This work is financially supported by the National Natural Science Foundation of China (51874135, 51904106) and Hundred Excellent Innovative Talents Support Program in Hebei Universities (No. BR2-214).

References

AHMADI, R., KHODADADI, D.A., ABDOLLAHY, M., FAN, M., 2014. Nano-microbubble flotation of fine and ultrafine chalcopyrite particles. *International Journal of Mining Science and Technology*. 24(7), 559–566.

- CHENG, P.F., SUN, W., HU, Y.H., LIU, R.Q., 2018. *Effect and mechanism of frothers on flotation of fine serpentine*. Journal of Central South University. 49(2), 261-267.
- DERJAGUIN, B.V., DUKHIN, S.S., RULYOV, N.N., 1984. *Kinetic Theory of Flotation of Small Particles*. Russ. Chem. Rev. 51(1), 51-67.
- HASSANZADEH, A., HASSAS, B. V., KOUACHI, S., BRABCOVA, Z., CELIK, M.S., 2016. *Effect of bubble size and velocity on collision efficiency in chalcopyrite flotation*. Colloid. Surface. A. 498, 258-267.
- JAMESON G.J., NAM, S., YOUNG, M.M., 1977. *Physical factors affecting recovery rates in flotation*. Miner. Sci. Eng. 9(3), 103-118.
- JIANG, Z.W., LI, Y.Z., 1993. *A theoretical study of the collision velocity between particle and bubble in flotation*. Journal of China University of Mining & Technology. 22(1), 73-78.
- JORGE, R., HEINZ, H., 1993. *The process of separation of fine mineral particles by flotation with hydrophobic polymeric carrier*. International Journal of Mineral Processing. 37(1), 109-122.
- KOUACHI, S., BOUHENGUEL, M., AMIRECH, A., BOUCHEMMA, A., 2010. *Yoon-Luttrell collision and attachment models analysis in flotation and their application on general flotation kinetic model*. Desalination. 264(3), 228-235.
- KOH, P.T.L., SMITH, L.K., 2011. *The effect of stirring speed and induction time on flotation*. Minerals Engineering. 24(5), 442-448.
- KRALCHEVSKY, P.A., BONEVA, M.P., DANOV, K.D., CHRISTOV, N.C., 2009. *Attraction between particles at a liquid interface due to the interplay of gravity- and electric-field-induced interfacial deformations*. Langmuir. 25(16), 9129-9139.
- NGUYEN, A.V., 1999. *Hydrodynamics of liquid flows around air bubbles in flotation: a review*. International Journal of Mineral Processing. 56(1-4), 165-205.
- NGUYEN, A.V., EVANS G.M., 2004. *Attachment interaction between air bubbles and particles in froth flotation*. Exp. Therm. Fluid. Sci. 28(5), 381-385.
- NGUYEN, A.V., NALASKOWSKI, J., MILLER, J.D., 2003. *A study of bubble-particle interaction using atomic force microscopy*. Minerals Engineering. 16(11), 1173-1181.
- NGUYEN, A.V., EVANS, G.M., 2004. *Attachment interaction between air bubbles and particles in froth flotation*. Experimental Thermal and Fluid Science. 28(5), 381-385.
- RAHMAN, A., AHMAD, K.D., MAHMOUD, A., FAN, M.M., 2014. *Nano-microbubble flotation of fine and ultrafine chalcopyrite particles*. International Journal of Mining Science and Technology. 24(4), 559-566.
- SCHULZE, H.J., 1989. *Hydrodynamics of bubble-mineral particle collisions*. Mineral Processing and Extractive Metallurgy Review. 5(1-4), 43-76.
- SHAHBAZI, B., REZAI, B., JAVAD KOLEINI, S.M., 2010. *Bubble-particle collision and attachment probability on fine particles flotation*. Chemical Engineering and Processing. 49(6), 622-627.
- SHI, R.D., GRIFFIN, W.L., O' REILLY, S.Y., HUANG, Q.S., LIU, D.L., GONG, X.H., CHENG, S.S., WU, K., YI, G. D. 2015. *Ophiolitic Chromitites Originated from Ancient SCLM*. Acta. Geol. Sin-Engl. 89(2), 84.
- SIVAMOHAN, R. 1990. *The problem of recovering very fine particles in mineral processing-A review*. International Journal of Mineral Processing. 28(3), 247-288.
- SONG, S.X., LI, C.G., CUI, H. S., 2007. *Theory and application of fine-grained mineral flocs flotation*. Minerals Engineering. (5), 4-9.
- TIAN, J., XU, L.H., YANG, Y.H., LIU, J., ZENG, X.B., DENG, W. 2017. *Selective flotation separation of ilmenite from titanite using mixed anionic/cationic collectors*. International Journal of Mineral Processing. 166, 102-107.
- WANG, X.L., REN, S.L., FU, Y.N. 2016. *Three-dimensional orbit and physical parameters of HD 6840*. Res. Astron. Astrophys. 16(2), 1-6.
- WANG, W., ZHOU, Z., NANDAKUMAR, K., XU, Z., MASLIYAH, J.H. 2003. *Attachment of individual particles to a stationary air bubble in model systems*. International Journal of Mineral Processing. 68(1), 47-69.
- WANG, W., ZHOU, Z., NANDAKUMAR, K., XU, Z., MASLIYAH, J.H. 2003. *Effect of surface mobility on the particle sliding along a bubble or a solid sphere*. Journal of Colloid and Interface Science. 259(1), 81-88.
- WU, H.Q., TIAN, J., XU, L.H., FANG, S., ZHANG, Z.Y., CHI, R. 2018. *Flotation and adsorption of a new mixed anionic/cationic collector in the spodumene-feldspar system*. Minerals Engineering. 127, 42-47.
- ZHANG, T., QIN, W.Q., YANG, C.R., Huang, S.P., 2014. *Floc flotation of marmatite fines in aqueous suspensions induced by butyl xanthate and ammonium dibutyl dithiophosphate*. Transactions of Nonferrous Metals Society of China. 24(5), 1578-1586.